Acoustic Modem for Micro AUVs: Design and Practical Evaluation

Christian Renner[*]
Research Group smartPORT
Hamburg University of Technology, Germany
christian.renner@tuhh.de

Alexander J. Golkowski
Institute of Computer Engineering
University of Lübeck, Germany

ABSTRACT

The recent development of small, cheap AUVs such as MON-SUN and Hippocampus enables a plethora of applications for underwater inshore monitoring. Among these are the detection of pollution sources in ports, water-quality monitoring in lakes, and the support and protection of divers in context of disaster management. These tasks profit from online reporting and controlling as well as swarm interaction between the AUVs. For this purpose, communication is required. In this paper, we present a prototype of an acoustic modem that is (i) small enough to be carried by micro AUVs in the sub 10 L class, (ii) consumes little enough energy to not diminish operation times of its host, (iii) comes at an attractive unit cost of less than € 600, and (iv) can reliably communicate at distances of 50 m and more. Due to its modular build, the modem can be easily customized and is hence suitable as research platform to analyze, e.g., MAC and routing protocols. We present results of detailed real-world studies of its communication range, packet reception rate, and ranging accuracy.

CCS Concepts

•Hardware → Wireless devices; •Computer systems organization → *Embedded systems;* Robotic autonomy;

Keywords

acoustic, underwater, communication, AUV, swarm

1. INTRODUCTION

Wireless networked sensing has already conquered many application domains over the last two decades and is currently stretching out to the field of inshore and coastal underwater monitoring and control. Starting from stationary underwater sensor networks [11, 13], a recent focus on cooperative, autonomous, mobile underwater robot swarms

---

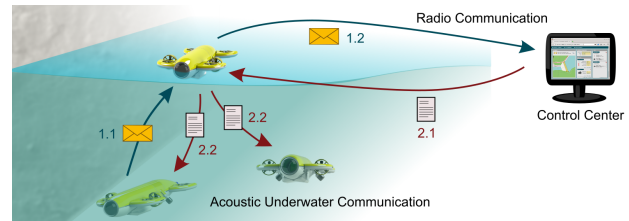[*]Work partly performed at University of Lübeck.

Figure 1: Potential application scenario for underwater swarms with a mobile relay station at the surface to enable fast response times without the need for surfacing of each robot.

[20, 16, 10, 5] has evolved in both academia and industry. Novel miniature mobile underwater robots with lengths well below 1 m and a unit cost between some hundred and a few thousand Euros have become available [14, 10, 12, 18]. Due to their size and low cost, these robots are frequently called micro autonomous underwater vehicles (μAUV).

These μAUVs ultimately enable automated, unsupervised environmental underwater inshore monitoring, inspections, and even interaction with the environment. Practical applications range from automated water-quality monitoring over inspections of bridges and wind parks to supporting divers in dangerous missions. Specific needs we identified when interviewing local administration in Hamburg are

- the timely detection of health hazards for the public,
- bio-hazards caused by oil leaks and pollutant introduction by ships or industrial equipment,
- examination of ship hulls, and
- disaster management support.

These tasks typically require fast reaction times and massively profit from collaboration of multiple robots. Figure 1 illustrates a possible scenario, in which two μAUVs perform an underwater monitoring task and report their measurements via a relay station at the surface to a control center. The latter may send instructions back to the μAUVs. A great advantage of such a cooperation is that robots performing an underwater task do not have to surface in order to communicate with the control center.

In consequence, underwater communication is a mandatory requirement. Since radio waves suffer from heavy absorption of the medium and the visibility in many waters is poor, only acoustic communication appears suitable. Unfortunately, we found that available acoustic modems [4, 7, 25, 24, 22, 19, 3, 9, 15, 8] cannot be easily integrated in μAUVs such as MONSUN [14] or Hippocampus [10] with tight constraints on size, battery capacity, modifiability, and cost (we

elaborate on this in Sect. 5). Furthermore, real-world experiments involving acoustic communication—as, e.g., carried out in [6, 17]—are essential for developing and assessing practical MAC and routing protocols as well as distributed underwater localization and swarm algorithms. However, there is a lack of practical experience regarding their use and performance in μAUVs. For these purposes, relatively inexpensive, customizable, and easily reproducible acoustic modems are required, yet not available.

We therefore designed and built an acoustic modem for underwater communication that serves two purposes. First, it is tailored to the particular needs of μAUVs. Second, it simplifies and enables real-world experiments in the domain of autonomous μAUV swarms and their communication. We discuss the design decisions and architecture of our modem, including both hard- and software aspects, with particular focus on the modularity and extensibility of our design. We present the results of an extensive evaluation of the hardware and real-world experiments to showcase the performance of the whole device in terms of communication range, packet reception rates, and ranging accuracy. Finally, we comment on future improvements and modifications of our modem and point out our follow-up research.

2. SYSTEM DESIGN

Next, we explain our fundamental considerations, the communication architecture, and its hardware implementation.

2.1 Considerations and Design Choices

The hardware/software co-design of an acoustic modem has an inherently large design space. However, our main objective was to design a low-power, low-cost, miniature yet reliable device to enable underwater communication between μAUVs such as MONSUN [14] of up to 100 m. In addition, we wanted to maintain a high customization potential and configurability. The latter preserves the possibility to tweak bits and pieces during the design phase—it is easier to change a few lines of code than to redesign and rebuild a circuit board (several times)—plus it allows the user (i.e., the researcher) to extend and customize the modem.

We hence decided to implement as much functionality in software as possible and opted for a microcontroller (μC) as processing core, as it offers a good trade-off between versatility and low power consumption. To keep the design and use simple, we abstained from adding a DSP or FPGA. We also think that computer scientists, researchers, and students are most experienced with μC programming, hence reaching a large group of potential users. Our results in Sect. 3.1 show that consumption is still very low and we were able to implement all required real-time functionality. All coding- and modulation-related functionality is therefore realized in software, leaving a light burden of analog filtering and signal amplification as hardware realizations. This approach also keeps the effort for assembly (soldering) and part costs low.

As pointed out in several research articles (e.g., [23, 26]), the underwater acoustic channel is affected by several sources of interference and frequency-dependent attenuation. Fading leads to signal level differences of 40 dB between ranges of 1 m and 100 m, requiring an adjustable amplifier gain. In shallow water, multi-path propagation is a severe problem due to heavy reflections at the surface. Particularly at short distances of a few meters, (surface) echos lead to inter-symbol and even intra-symbol interference, so that coun-
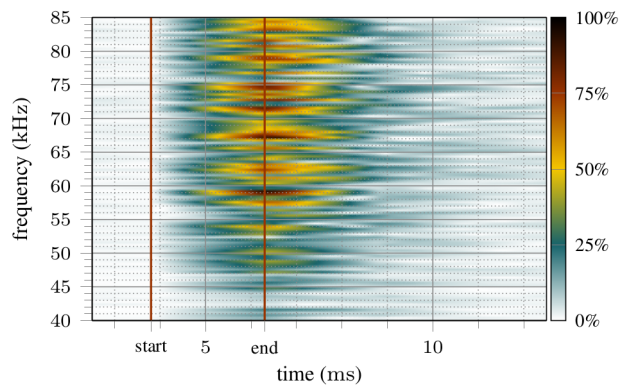

Figure 2: Received signal intensities (amplitudes) of a frequency sweep of 2.5 ms long sine waveforms (equal transmit levels) in a distance of 5 m at 70 cm depth. On an ideal (unity-gain, free-field) channel, (receive) intensities would be equal with a maximum indicated at the time labeled "end" (the maximal value of cross correlation occurs at the end of the received waveform/symbol).

termeasures are needed. Figure 2 illustrates the effect of constructive and destructive interference due to multi-path propagation for a frequency sweep. Repeated sweeps show changing results due to surface waves. μAUV movement leads to a frequency shift due to the Doppler effect; e.g., a 75 kHz signal will be shifted by 200 Hz if two μAUVs move at 2 m/s in opposite direction. At rather short communication ranges up to 100 m and frequencies up to 100 kHz, absorption is below 1 dB in fresh water and at most 4 dB in sea water [26]—it is hence negligible.

2.2 Acoustic Communication Architecture

To enable acoustic underwater communication for μAUVs and to showcase the function of our modem, we implemented a reference communication stack, ranging from modulation to encoding. We discuss the stack subsequently with reference to the challenges in Sect. 2.1 and evaluate it in Sect. 4.

We implement orthogonal binary frequency shift keying (BFSK). It is well suited for communication of moving devices and can be realized without tight synchronization between receiver and sender, keeping hard- and software less complex. To account for the Doppler effect at speeds of only a few m/s, frequency spacing is 400 Hz with a symbol duration of 2.5 ms to achieve orthogonality, which is particularly useful to counter the typical echos on the channel. Signal composition and detection are entirely done in software based on a look-up table and incoherent detection through cross correlation during reception. To elevate the data rate, M bits (currently up to 4) can be transmitted per symbol, which hence consists of M superimposed sine waveforms.

Amplitudes of these symbol components are scaled by the sender to achieve equalized levels (amplitudes) at the receiver. We hence compensate the non-flat transfer function of the filter and hydrophone; we will refer to this as *gain compensation*. For this purpose, we combined the results from Sect. 3.2 with the transfer function of the used AS-1 hydrophone (cf. Sect. 2.3) to obtain the corresponding coefficients that are applied during modulation.

To counter frequency- and time-dependent attenuation due to multi-path propagation, we apply a spread spectrum mechanism. Each bit is repeated on S carriers, and the

receiver only uses the detected bit with highest level (amplitude) of a spread series. Additional techniques to address inter-symbol interference are frequency hopping (FHSS) with a sequence length of five (to discard echoes of up to $10\,\mathrm{ms}$) and (short) guard intervals between symbols to reduce the impact of imprecise synchronization. We also use extended Hamming codes, interleaving, and two checksums (CRC-8 for the header and CRC-16 for the payload, cf. Sect. 2.4).

Per-packet synchronization is achieved through a preamble of P symbols. Rather than simply alternating between two sine waveforms of different frequencies (space and mark), we address time- and frequency-dependent attenuation as follows: Each symbol is made up of two sine waveforms (typically a higher and a lower frequency from the used band) that are only reused every fourth symbol. These frequencies are not used for data transmission.

This setup gives a net data rate of up to $800\,\mathrm{bit/s}$ for $S = 1, M = 4$ (a maximum of $1600\,\mathrm{bit/s}$ is achievable without Hamming encoding) and requires a baseband bandwidth of $25\,\mathrm{kHz}$. Choosing the frequency band depends on several factors. Firstly, the used AS-1 hydrophone suggests an upper band limit of around $100\,\mathrm{kHz}$, where the transmit level is highest, before it cuts off. Secondly, noise from ships, animals, and the AUVs' thrusters resides in sub or low kHz regions, so that a high frequency is better. Thirdly, signal sampling and processing during de-/modulation on the AVR32 restricts the signal frequency to $75\,\mathrm{kHz}$. We hence chose the band from 50–$75\,\mathrm{kHz}$ for communication. In this setup, signal transmission runs at a sampling rate of $150\,\mathrm{kHz}$, whereas we have to make use of undersampling at $50\,\mathrm{kHz}$ in receive mode, which requires a very narrow band pass.

2.3 Hardware Implementation

We chose an AVR32 μC with a maximum clock speed of $66\,\mathrm{MHz}$ [2] to provide sufficient computing resources at an affordable price combined with low power consumption. One standalone, low-power DAC and ADC each ensure high analog signal quality and low sampling noise. To simplify debugging and evaluation, 12 GPIO pins are accessible through pin headers, of which 4 are connected to low-current LEDs. These core components are placed on a mainboard with two switched voltage converters to supply the microcontroller ($3.3\,\mathrm{V}$) and the analog receive circuitry (we picked $5\,\mathrm{V}$ as a trade-off between low power consumption and good SNR). The mainboard also provides a $2.5\,\mathrm{V}$ reference voltage for the analog receive chain to work with a single-ended supply. Modularity of analog signal processing (receiver-side) and power amplification (sender-side) is ensured by a modular design, in which up to four analog filter stages can be connected to the mainboard. All stages have a common pin layout, including the supply, the bias, analog signal input and output, and four μC GPIOs. The power amplifier is connected to a single μC GPIO (to disable the amplifier when it is not needed), the main power supply, and signal input and output. Communication with the host (μAUV) is serial. While the current layout of the mainboard meets the form factor of the MONSUN robot [14] due a common research project, the modem can be used standalone and we are currently developing an entirely independent layout.

We decided for an Aquarian Audio miniature AS-1 hydrophone [1] acting as both sender and receiver. It has a very small size ($\varnothing 12\,\mathrm{mm} \times 40\,\mathrm{mm}$), an affordable price of €400, and was readily available in small numbers. More-

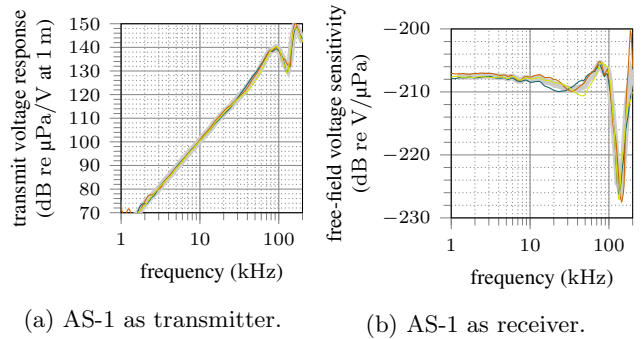(a) AS-1 as transmitter.   (b) AS-1 as receiver.

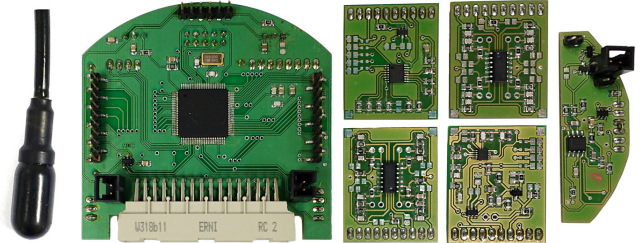Figure 3: Transmit and receive characteristics of three Aquarian Audio AS-1 hydrophoness [1].

Figure 4: Acoustic modem prototype (left to right, top to bottom): hydrophone, mainboard, amplifier, high pass, low pass, driver with pre-amplifier, power amplifier.

over, it offers a high bandwidth of almost $100\,\mathrm{kHz}$ with a flat frequency response and a relatively high, linear transmit voltage sensitivity (see Fig. 3).

The power amplifier converts the DAC output to a maximum amplitude of $16\,\mathrm{V}$ at $50\,\mathrm{mA}$. A 2nd order low pass serves as reconstruction filter. The amplifier can be disabled, when it is not needed, leading to a negligible µW power consumption. Our current design makes use of all four stages of the receive filter chain. It consists of an electronically adjustable pre-amplifier ranging from $40\,\mathrm{dB}$ to $64\,\mathrm{dB}$ in $6\,\mathrm{dB}$ steps with a JFET hydrophone driver. An 8th order high and low pass each in Sallen-Key topology ensure a very selective filter, which is required due to the high overall amplification needed and the undersampling. Corner frequencies are at $50\,\mathrm{kHz}$ each, where the low pass compensates the resulting attenuation in the pass band by a $6\,\mathrm{dB}$ gain. An electronically adjustable amplifier ($4\,\mathrm{dB}$ steps from 6 to $38\,\mathrm{dB}$) is the last element of the chain. In conjunction with our power amplifier and the hydrophone, the amplification range is designed to allow communication from $1\,\mathrm{m}$ up to $100\,\mathrm{m}$.

Figure 4 shows all parts of one of our modem prototypes. The assembled prototype has a size of $7\,\mathrm{cm} \times 7\,\mathrm{cm} \times 4\,\mathrm{cm}$.

2.4 Communication Interface

Communication between the host (μAUV) and the modem is packet-based (UART). Each packet consists of a 2-byte header ($1\,\mathrm{B}$ packet type, $1\,\mathrm{B}$ payload length) and the corresponding payload. Packets sent to the modem are immediately put on the acoustic channel (after encoding, checksum addition, etc.), and packets received by the modem are immediately forwarded to the host. Addressing, back-offing etc. are done by the host or can be implemented on top of the current communication stack.
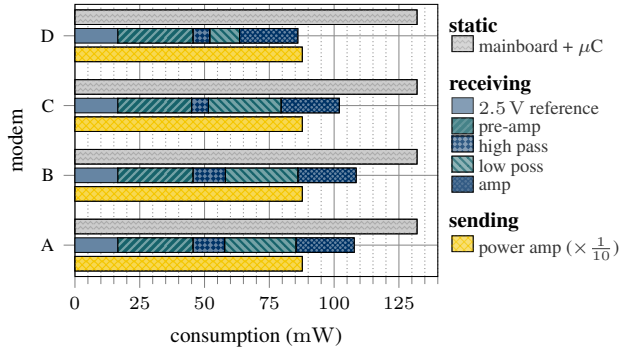
Figure 5: Consumption split of four modem prototypes. Note the different scale for the power amplifier.

We defined a set of special packets (types) that are processed by the modem (and not transmitted on the acoustic channel). They act as commands to read out values, such as the current noise level or packet statistics, and to change parameters such as the amplifier gain, S, and M.

3. HARDWARE EVALUATION

Before analyzing communication performance metrics of our acoustic modem, we assessed and validated the hardware with particular interest in consumption and quality of the receive filter chain and power amplifier.

For the measurements in this section, we built five modems named A through E. All modems are equally equipped with the following exceptions: Modem C uses a lower-power high pass, and modem D uses a lower-power high and low pass. We made these modifications to assess the quality and impact of different components (mainly operational amplifiers).

3.1 Power Consumption

A major design aspect was to achieve low overall power consumption, so that our acoustic modem could be powered by either a small, dedicated (rechargeable) battery or from the μAUV's main supply without affecting the mission time. To understand the power consumption in more detail, we analyzed the components (mainboard, receive filter chain stages, power amplifier) of four modems individually. We measured the supply voltage directly and the current consumption through a $1\,\Omega$ shunt. Values for the receive filter parts were measured at their inputs to be able to sum up the component splits. Overall consumption will be roughly 10% higher due to the DC-DC-converter. All measurements (except for the mainboard) were repeated for different input signal frequencies (from 50 kHz to 75 kHz) at amplitudes leading to a maximum output signal. Measurements for the power amplifier and receive pre-amplifier were conducted with a connected AS-1 hydrophone.

The results are displayed in Fig. 5. Figures for the receive and send circuitry are averaged over the different signal frequencies. In receive mode (power amplifier switched off), the overall consumption ranges from 225 mW to 252 mW. Using lower-power filters reduces the consumption of the filter chain by 27%; however, we favor the combination of the higher-power high pass and the lower-power low pass, as the lower-power high pass increased the overall noise level. In send mode, overall consumption is raised by 880 mW on av-

erage. Here, higher frequency signals consume additional power, since the conductance of the AS-1 increases.

With these figures and a typical mission duration of up to 5 h, it is possible to run our modem in listening/receiving mode with a LiPo-battery rated at 11.1 V with as low as 110 mA h capacity. When using the main supply of an μAUV such as MONSUN with a 4.5 A h LiPo-battery at 11.1 V, the modem will only use 2.5% of its host's energy budget within a mission, so that mission duration would be affected insignificantly. In a scenario with one transmission every minute—this is roughly equal to 5% transmit time—the latter figure rises to 3%. Equally, a standalone battery with 130 mA h capacity would be required.

3.2 Gain and Filter Quality

We assessed the static and transient behavior of the analog receive filters and the power amplifiers. We measured every filter and amplifier module separately plus five complete chain setups. We supplied the modules with one of the modem mainboards and ran a frequency sweep from 400 Hz to 200 kHz in steps of 400 Hz up to 100 kHz and 10 kHz for the remaining range. All signals had a length of 2.5 ms (a symbol duration) with a leading and trailing silence of 0.5 ms.

Depending on the module type, we used different DC offsets and input signal amplitudes to achieve a maximum output level. To maintain comparable input signal resolutions in the face of the large gain of the amplifier modules, we attenuated the signal through a voltage divider between frequency generator and module input. For the pre-amplifier, we simulated the hydrophone through a series capacitor between the voltage divider and the pre-amplifier input[1]. For the amplifier, we used a passive high pass biasing circuit to achieve the required 2.5 V input DC level. The cut-off frequency of this circuit was 160 Hz, so that input signals roughly above 1 kHz were not affected.

Measurements were performed with a TiePie Handyscope HS-3 USB signal generator and two-channel oscilloscope. Signals were generated with a 14 bit ADC resolution, a maximum voltage range of ± 8 V, and a sampling frequency of 1.5626 MHz. Signals were recorded with the same setup except for a voltage range of ± 10 V. We used the first channel of the HS-3 to record the generated signal and the second channel to measure the output of the filter/amplifier module. To assess the quality of the modules, we derived theoretical models for their ideal frequency response.

From these measurements, we calculated the frequency responses (transfer functions) displayed in Fig. 6. They show that the part variation is very low in most cases. Largest variations up to 2 dB in the communication frequency band are noted for the pre-amplifier in Fig. 6a. This is caused by the rather large tolerances of the input JFET. Here, we deliberately traded off a higher gain and signal to noise ratio for a higher variation. We also noted a 1 dB variation for the power amplifier of modem E (see Fig. 6e) compared to its four siblings, for which there is no particular explanation.

The majority of measurements follow the corresponding ideal behavior closely. Exceptions are found for higher gain setups of the pre-amplifier (Fig. 6a) and amplifier (Fig. 6d), since those setups operate closely at design specifications; in particular, they exploit the gain-bandwidth product of the operational amplifiers to a maximum. We did this de-

---

[1]In a first-order approximation, a hydrophone is an ideal voltage source with a capacitor as output impedance.
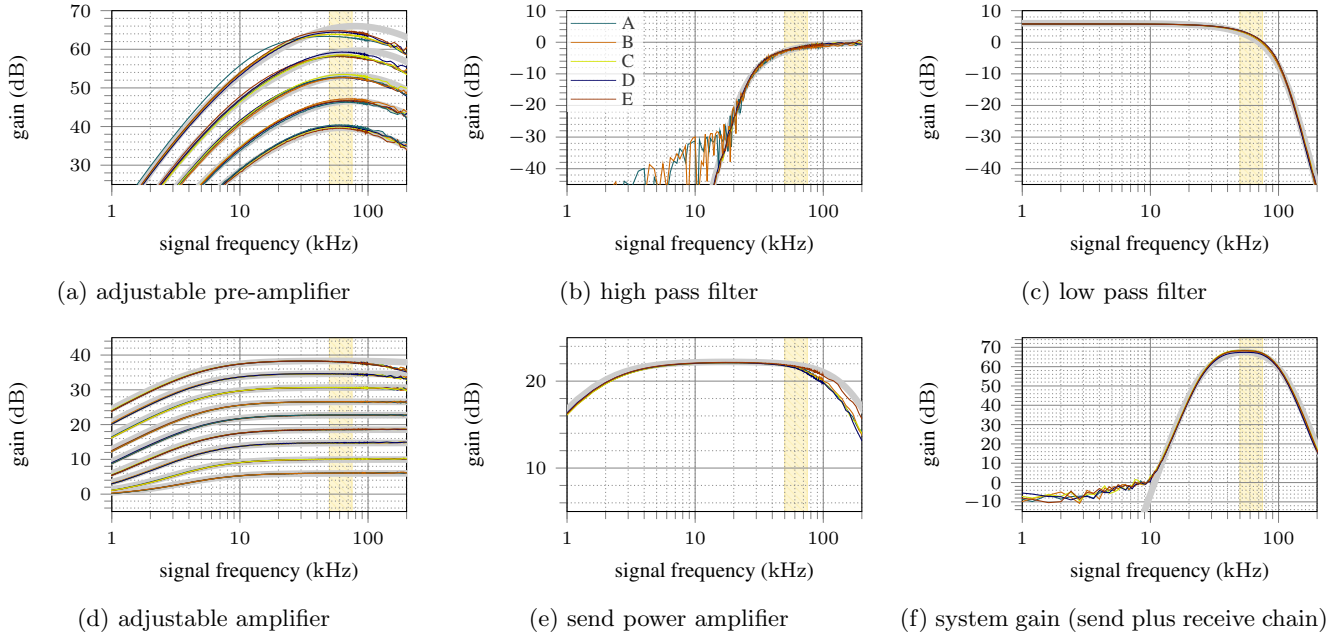
Figure 6: Gain of individual filter stages (receiver), power amplifier, and total gain (without hydrophone). All plots show the results of four prototypes, bold light gray lines indicate ideal behavior (without parasitic effects). System gain was measured in the lowest gain setup. The light yellow hashed area represents the frequency band used for communication.
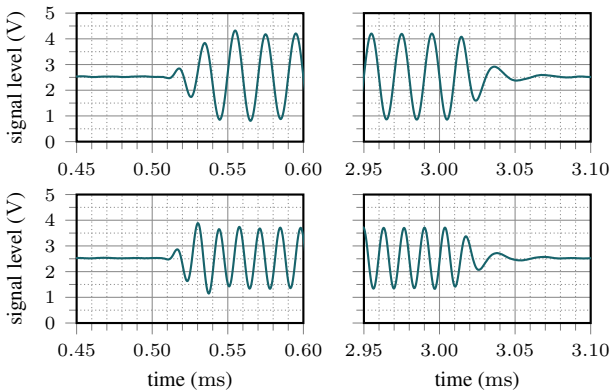

Figure 7: Analysis of the transient response of the receive filter chain for a 50 kHz (upper row) and a 74 kHz sine signal. The sine signals last from 0.5 ms to 3.0 ms.

liberately to achieve the largest possible gain with a single operational amplifier.

However, the variation of the entire system gains in Fig. 6f is below 1 dB and falls well within the ideal behavior, hence indicating a reliable, reproducible hardware. We'd like to point out here that the large deviation from the ideal behavior for low frequencies (<10 kHz) is due to the restricted measurement range.

In addition to the gain, we also measured the group delay but omit the plots due to space limitations and low additional insight. All group delays are within a few tenth of microseconds and exhibit a very low slope within the communication frequency band.

To wrap this study up, we analyzed the transient behavior of the receive filter chain. We noted a slight overshoot ten-

dency and short settle times. Figure 7 shows the response to two sine waveforms of a symbol's duration. The behavior is virtually unchanged across the communication frequency band. Settle times are almost constant and overshoots are small, so that no countermeasures are required.

4. REAL-WORLD EXPERIMENTS

Finally, we evaluated the real-world communication performance of our modem on several days in a small marina at the Ratzeburger Lake in early spring when there were no boats. We choose this environment due to its easy accessibility and the presence of boardwalks leading roughly 50 m into the water, so that we could conduct experiments in a realistic scenario for inshore μAUV swarms. All experiments were conducted with the following setup and methodology. We placed two modems (A and B) on different boardwalks at distances of 9.5 m, 24.8 m, and 45 m. Their hydrophones were let into the water at half the water depth of 1.5 m without particular orientation. We ensured line-of-sight between the hydrophones despite obstacles such as wooden posts, partial ground plant cover, and small areas of reed. Due to the shallow water and surrounding reed, we could not perform realistic experiments at larger distances.

To investigate the plain performance up to layer 2 of the ISO/OSI model, we did not use any kind of medium access control (MAC). In particular, this means that a packet is sent exactly once by the modem, there are no acknowledgments and no retries.

If not otherwise noted, the modems are configured to send $M = 4$ bits per symbol and use a spreading ratio $S = 3$ and a preamble of $P = 16$ symbols. Gain compensation is enabled. We chose this setup due to promising early experiments.

At this point, we'd like to point out that experiments with acoustic communication are strictly limited by the factor time. Due to the very low speed of communication (a 64 B

(a) 24.8 m distance, no gain compensation

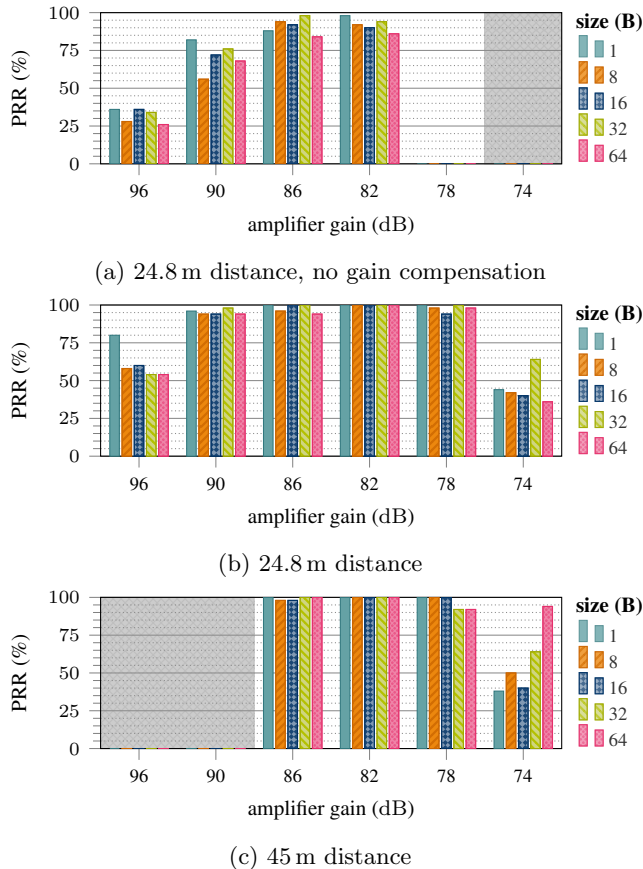(b) 24.8 m distance

(c) 45 m distance

Figure 8: Packet Reception Rate (PRR) vs. amplifier gain and payload size. Grayed out areas indicate untested scenarios.

packet takes more than 2 s on the channel), the number of experiments that suit into a day is rather small. Due to environmental changes that immediately affect the acoustic channel (waves, suspended particles), results from different days may not be comparable.

4.1 PRR vs. Payload Size

As a first experiment, we evaluated the influence of distance, payload size, and gain compensation on the packet reception rate (PRR). At distances of 24.8 m and 45 m, we sent 50 packets each of payload sizes from 1 B to 64 B from modem A to modem B at various amplifier gain levels. At 24.8 m, we also ran a series of measurements with disabled gain compensation. Packets were sent in intervals of 2 s to avoid any influence of echos from previous packets.

A detailed study of the results is depicted in Fig. 8. The first and main observation is that PRR is as high as 100 % for a broad, overlapping range of amplification gains. This implies that there is a possible gain setup working at a large range of distances and that trimming the gain to a specific value is not absolutely necessary. A cross-comparison between recordings on different days with different weather conditions produced similar results with a slight shift of gain values by roughly half a gain step (2 dB).

The second observation is that payload length does not have a notable impact on PRR; we believe that variations and outliers will be reduced for an increased number of pack-
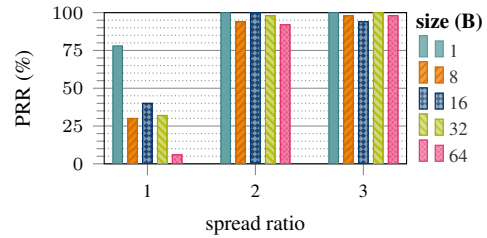

Figure 9: Influence of spread ratio S on PRR at a distance of 24.8 m with gain compensation and 78 dB amplifier gain.

Table 1: Detailed receive statistics

Spread	Syncs	Received	CRC Err.	Decode Err.
1	248	93	6	149
2	248	242	0	6
3	247	245	0	2

ets used for analysis. This is an extremely important finding, because long packets occupy the channel for more than 2 s— a time in which massive changes on the channel are likely. The combination of countermeasures described in Sect. 2.2 lead to this positive result.

The third observation is that gain compensation has a very positive impact. This is an expected result, because we explicitly enforce equal receive amplitudes (in the communication band) in absence of interference (echos, etc.). Therefore, the chance of suppressed signal parts (frequencies) is more evenly spread over the entire (communication) frequency range. As a result, the effect of spreading (repeating one data bit on multiple frequencies) is pronounced. Without gain compensation, higher frequencies typically have higher amplitudes (due to the AS-1 transmit characteristic), so that destructive interference leads to a higher risk of erroneous decoding.

However, the figures also indicate that the transition zone between a high and low PRR is relatively narrow. One major reason is that synchronization simply fails when the signal is becoming too weak. This is supported by the fact that once a synchronization is successful, a packet is likely received. On the contrary, too large a gain will result in clipping and hence reduces the PRR, because higher frequency parts cannot be detected any longer, leading to an aborted synchronization or high bit error rates.

4.2 Spreading and Bit Concurrency vs. PRR

At this point, we study the impact of the spread ratio S and the number M of bits per symbol on PRR. Both parameters trade off a high PRR vs. a faster data rate.

First, we examined the influence of the spread ratio. At a distance of 24.8 m, we repeated the PRR experiments from Sect. 4.1 for spread ratios of 2 and 3 at a fixed gain of 78 dB. The results are depicted in Fig. 9 and produce two main findings. First, a spread ratio of 2 already improves the PRR significantly, because every bit is transmitted on two different frequencies, hence decreasing the chance of erroneous detection in case of destructive inference. Since a spread of 3 does not add any improvement, we conclude that the chance of destructive interference on more than one frequency is already low enough. Second, payload size influences the PRR for $S = 1$. This may be caused by echos, that increase the
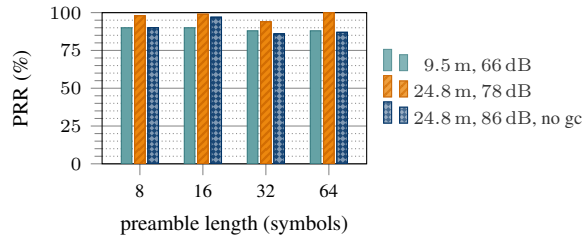
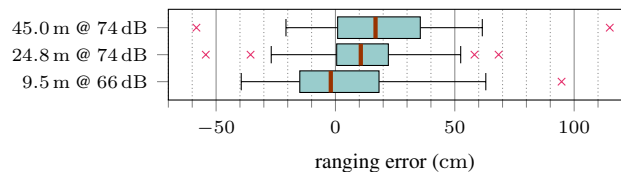Figure 10: Influence of preamble length on PRR.

Figure 11: Boxplot of ranging errors based on two-way time-of-flight assessment. The boxplot shows the median, upper and lower quartiles. Maximum whisker length is 1.5 of the box length, outliers are marked. Errors are calculated from the estimated (ranged) distance and the actual distance between the modems.

likelihood of wrong detection on longer packets, if a data bit is only transmitted on one frequency. While the modem was able to detect a packet start in almost all cases, see Table 1, the number of decode errors (i.e., more than one bit error per symbol) increased dramatically for $S = 1$. An important result of this analysis is that it is possible to transmit ultra short packets without spreading while longer packets profit from a spread ratio of at least $S = 2$.

In addition, we repeated the experiments for $M = 2$ bits per symbol without any notable insight. In fact, a lower number of bits per symbol will increase the SNR, or amplitude of the individual frequency parts within a symbol, respectively, at the same gain. This will result in a higher communication range. We ran a short experiment at a distance of 75 m to validate this behavior. With an amplifier gain of 90 dB and $S = 3$, we were able to receive 41 short packets for $M = 2$, whereas we only received 24 packets for $M = 4$. As an extension of our findings for the 24.8 m distance, we found that using $S = 2$ for two concurrent bits per symbol reduced the number of received packets to 24. We trace this behavior back to the increased distance and obstacles (reed, wooden posts) in between sender and receiver.

4.3 Preamble Length vs. PRR

From a statistical point of view, the preamble length influences the quality (precision) of synchronization. In particular, a longer preamble should improve precision. A better synchronization leads to more reliable detection of the signal frequencies, because the overlap for correlation is improved; i.e., the correlation window and the actual symbols of the signal are tighter aligned. We studied the impact of the preamble length on the PRR by sending 100 empty packets from modem A to B. The results shown in Fig. 10 do not reveal a notable influence of the preamble length in any of the three cases. As there was no physical connection between the two modems possible during our experiments and we did not have access to high-resolution, synchronized clocks, we could not assess synchronization quality in more detail.

4.4 Ranging Accuracy

Finally, we evaluated the ranging accuracy of our modem by a simple time-of-flight, two-way ping-pong mechanism as a proof-of-concept analysis. In particular, modem A sent 100 short packets (pings) without payload to modem B, which in turn responded with a pong (no payload). The time difference between sending and receiving measured by modem A was logged to calculate the distance offline. We measured a water temperature of 8.9 °C and a depth of 70 cm, and we assumed a salinity of 0 ‰. These values yield a speed of sound of 1443 m/s according to [27], a distance resolution of 2.9 cm with a theoretical maximum error of 3.6 m (a symbol

duration). A typical μAUV will likely measure these values to determine the speed of sound during its normal operation, so that online ranging can be easily achieved.

We ran experiments with different amplifier gains, spread ratios, preamble lengths, and bit concurrency without a notable impact of these parameters. Figure 11 summarizes the results for different distances for the gain setup with most received pongs each (84, 100, and 90 at the displayed distances in increasing order). The figure suggests that ranging is (on average) particularly precise at small distances and deteriorates with distance. However, we were only able to measure the distances between the hydrophone cables at the water surface. It is likely that the actual distances varied from these values by several centimeters (due to bent cables and water current), leading to an error in ground truth of the same magnitude. The expressiveness of the results lies hence more on variation (from the median). The overall shape of the boxplots is similar, meaning that the distribution of errors is independent from the distance and the relative error thus decreases with distance. 50% of distance estimations deviate at most 20 cm from the median, implying a synchronization error within at most 8 samples. In many application scenarios (such as dam inspections, environmental monitoring), the achieved precision is sufficient for underwater localization.

5. RELATED WORK

In the last decade, several research groups and companies have designed and presented modems for acoustic underwater communication. We position our acoustic modem against the most prominent devices. A comprehensive and very recent study is also available in [21].

Commercial modems are off-the-shelf solutions and, in theory, only need a few wires, manual reading, and (usually serial) interfacing with the robot. However, their unit cost likely overshoots that of the host by a multiple, hence rendering them unattractive for (swarm) research; e.g., the Evologics S2C M HS [7] comes at roughly €8000 per unit. Our modem comes at €600 material cost plus assembly, which can be realized at very low costs at most research institutes. Other modems; e.g., the Teledyne ATM-903 [24], the Sonardyne uComm [22], and the AppliCon SeaModem [4]—are too large for easy integration in μAUVs. Our modem has been been particularly tailored to fit into MONSUN and will fit into Hippocampus, one of the smallest available μAUVs, in the next hardware iteration. The Tritech Micron [25] has an extremely low data rate of only 40 bit/s, likely hindering swarm communication. Our modem improves on the data rate by a factor of eight or more, depending on (soft-

ware) configuration. Another important fact is that there is typically no access to the firmware of commercial modems, rendering real-world experiments with, e.g., novel MAC protocols difficult, if not impossible.

Due to these issues, academia has produced quite a number of acoustic modems. However, they also have limitations, so that we finally decided to build our own modem for swarms of μAUVs. In comparison with our modem, the WHOI micro modem 2 [9] has a comparable consumption in receive mode, a higher consumption during transmission, but offers a hibernate mode below 1 mW. However, the micro modem is relatively large (1.6 times the length of our modem) for μAUVs and has a price comparable to the Evologics devices. Benson et al. use a homemade transducer for their UWmodem in [3]. While they achieve a very low unit cost of 50 $, our modem is based on an off-the-shelf transducer involving no extra handcraft. Their modem uses an FPGA as processing unit, whereas we rely on a μC. We chose this option to increase implementation comfort (cf. Sect. 2.1). Our modem consumes less power at comparable communication performance. Nowsheen et al. present a software-defined acoustic modem also based on an FPGA in [15] with the demodulator only being available in Matlab. The ITACA modem [19] is promising for static and mobile underwater, low-power networks. However, the used piezo-electronic transducer is highly directional and the communication performance w.r.t. bit or packet error rates is unclear.

6. CONCLUSION

Low-cost, low-power, and versatile acoustic modems are mandatory for underwater communication in μAUV swarms and associated research. Existing modems are typically too large, too expensive, or too restricted for these purposes. In this paper, we hence presented our design and implementation of an acoustic modem that ticks all boxes. Particularly its low unit cost and consumption, modular design, and extensibility make it an attractive alternative for underwater communication in low-cost μAUVs and swarm research.

We evaluated the hardware and communication performance of our modem in the laboratory and through real-world experiments. We achieved up to 100% PRR in distances up to 45 m in a broad range of amplification settings in shallow water, and we evaluated the influence of several communication parameters on reliability and data rate. Accurate ranging is also possible.

As follow-up work, we are planning a measurement campaign with moving MONSUN and/or Hippocampus μAUVs to evaluate PRR and ranging accuracy for underwater self-localization. To increase the communication range, we are currently investigating methods for automatic gain control. We also intend to carry out research on medium access control for μAUV swarms.

Acknowledgments

7. REFERENCES

[1] Aquarian Audio Products. Aquarian hydrophones. http://www.aquarianaudio.com. Accessed: 2016/07/26.

[2] Atmel Corp. Atmel AT32UC3A1512. http://www.atmel.com/devices/AT32UC3A1512.aspx. Accessed: 2015/12/01.

[3] B. Benson, Y. Li, R. Kastner, B. Faunce, K. Domond, D. Kimball, and C. Schurgers. Design of a Low-Cost, Underwater Acoustic Modem for Short-Range Sensor Networks. In *OCEANS*, Sydney, Australia, 2010.

[4] G. Cario, A. Casavola, M. Lupia, and C. Rosace. SeaModem: A Low-Cost Underwater Acoustic Modem for Shallow Water Communication. In *OCEANS*, 2015.

[5] V. Djapic, W. Dong, D. Spaccini, G. Cario, A. Casavola, P. Gjanci, M. Lupia, and C. Petrioli. Cooperation of Coordinated Teams of Autonomous Underwater Vehicles. In *IFAC*, Leipzig, Germany, 2016.

[6] M. W. Doniec, I. Topor, M. Chitre, and D. Rus. Autonomous, Localization-Free Underwater Data Muling using Acoustic and Optical Communication. In *ISER*, Quebec City, Canada, 2012.

[7] Evologics GmbH. Underwater Acoustic Modems. http://www.evologics.de/en/products/acoustics/. Accessed: 2016/07/26.

[8] L. Freitag, M. Grund, S. Singh, J. Partan, P. Koski, and K. Ball. The WHOI Micro-Modem: An Acoustic Communcations and Navigation System for Multiple Platforms. In *OCEANS*, 2005.

[9] E. Gallimore, J. Partan, I. Vaughn, S. Singh, J. Shusta, and L. Freitag. The WHOI Micromodem-2: A Scalable System for Acoustic Communications and Networking. In *OCEANS*, 2010.

[10] A. Hackbarth, E. Kreuzer, and E. Solowjow. HippoCampus: A Micro Underwater Vehicle for Swarm Applications. In *IROS*, Hamburg, Germany, 2015.

[11] J. Heidemann, M. Stojanovic, and M. Zorzi. Underwater Sensor Networks: Applications, Advances, and Challenges. *Phil. Trans. Royal Society–A*, 370(1958):158–175, 2012.

[12] Hydromea. Vertex AUV System Overview. http://hydromea.com/vertex_brochure.pdf. Accessed: 2016/08/01.

[13] J. Lloret. Underwater Sensor Nodes and Networks. *Sensors, SI on Underwater Sensor Nodes and Underwater Sensor Networks*, 13(9):11782–11796, 2013.

[14] B. Meyer, C. Renner, and E. Maehle. Versatile Sensor and Communication Expansion Set for the Autonomous Underwater Vehicle MONSUN. In *CLAWAR*, London, UK, 2016.

[15] N. Nowsheen, C. Benson, and M. Frater. A High Data-Rate, Software-Defined Underwater Acoustic Modem. In *OCEANS*, Sydney, Australia, 2010.

[16] C. Osterloh, B. Meyer, A. Amory, T. Pionteck, and E. Maehle. MONSUN II – Towards Autonomous Underwater Swarms for Environmental Monitoring. In *IROS*, 2012.

[17] K. Pelekanakis and M. Chitre. Robust Equalization of Mobile Underwater Acoustic Channels. *IEEE Journal of Oceanic Engineering*, 40(4):775–784, 2015.

[18] Riptide Autonomous Solutions. Micro-UUV. https://riptideas.com/micro-uuv/. Accessed: 2016/08/01.

[19] A. Sanchez, S. Blanc, P. Yuste, and J. J. Serrano. A Low Cost and High Efficient Acoustic Modem for Underwater Sensor Networks. In *OCEANS*, Santander, Spain, 2011.

[20] T. Schmickl, R. Thenius, C. Möslinger, S. Kernbach, T. Dipper, D. Sutantyo, J. Timmis, A. Tyrrell, M. Read, J. Hilder, C. Stefanini, L. Manfredi, S. Orofino, J. Halloy, and A. Campo. CoCoRo - The Self-aware Underwater Swarm. In *SASO*, Ann Arbor, MI, USA, 2011.

[21] S. Sendra, J. Lloret, J. M. Jimenez, and L. Parra. Underwater Acoustic Modems. *IEEE Sensors*, 16(11):4063–4071, 2016.

[22] Sonardyne. uComm – Acoustic Modem. http://www.sonardyne.com/images/stories/datasheets/Sonardyne_8260_uCOMM.pdf. Accessed: 2016/08/01.

[23] M. Stojanovic and J. Preisig. Underwater Acoustic Communication Channels: Propagation Models and Statistical Characterization. *IEEE Comm. Mag.*, pages 84–89, 2009.

[24] Teledyne Benthos. ATM-903 series (OEM). http://teledynebenthos.com/product/acoustic_modems/903-series-atm-903. Accessed: 2016/08/01.

[25] Tritech Intl. Ltd. Micron Data Modem – Acoustic Modem. http://www.tritech.co.uk/product/micron-data-modem. Accessed: 2016/08/01.

[26] R. J. Urick. *Principles of Underwater Sound 3rd Edition*. Peninsula, 1996.

[27] G. S. K. Wong and S. ming Zhu. Speed of Sound in Seawater as a Function of Salinity, Temperature and Pressure. *Acoustic Society America*, 97:1732–1736, 1995.